



Optimal Bayesian Neural Network based Decision Support System for Mitotic Nuclei Detection on Histopathologic Imaging

Ali Allouf^{1,*}

¹University of Calabria, Department of computer engineering modelling, electronics and systems, Italy

Email: Ali1allouf@gmail.com

Abstract

A Decision Support System (DSS) for the recognition of mitotic nuclei (MN) on the histopathological image (HI) aids pathologists in cancer diagnoses by automating the MN detection, a key indicator of tumor proliferation and cell division. Leveraging innovative image processing and machine learning (ML) algorithms, such a system can accurately detect MN, which are crucial indicators of cell division and tumor proliferation. By automating these processes, pathologists can focus more on complicated diagnostic tasks while ensuring efficient and consistent analysis. ML approaches, comprising support vector machines (SVMs) or convolutional neural networks (CNNs) can be widely applied for the classification task. These techniques learn from annotated data to accurately discriminate between mitotic and non-MN. Incorporating these technologies into pathology workflow facilitates research efforts in oncology for improved treatment strategies, enhances diagnostic accuracy, and reduces variability among observers. This study presents an Optimal Bayesian Neural Network based Decision Support System for Mitotic Nuclei Detection (OBNN-DSSMND) technique on Histopathologic Imaging. The goal of the OBNN-DSSMND technique is to detect the mitotic and non-mitotic cells on the HIs. In the initial phase, the OBNN-DSSMND technique undergoes the bilateral filtering (BF) technique to preprocess the input images. Next, the OBNN-DSSMND technique involves a feature fusion process encompassing SqueezeNet, DenseNet, and VGG-19 models. Meanwhile, the hyperparameter selection of the DL models is performed by using the Archimedes Optimization algorithm (AOA). For mitotic nuclei detection, the OBNN-DSSMND technique applies a BNN classifier, which recognizes the presence of mitotic and non-mitotic cells on the HIs. The experimental assessment of the OBNN-DSSMND approach was examined utilizing a benchmark image dataset. The widespread simulation analysis reported that the OBNN-DSSMND technique achieves better results than other techniques.

Keywords: Breast Cancer; Mitotic Nuclei Detection; Decision Support System; Bayesian Neural Network; Histopathologic Image

1. Introduction

Breast cancer (BC) is a common cancer that mainly affects the lives of women all over the world. BC grows and changes due to anomalies in the rate of cell proliferation [1]. The mitotic activity index (MAI) has frequently been utilized to evaluate the change in the rate of cell proliferation [2]. MAI was defined as a ratio of cells below separation to the entire cell population, and it was assessed by including mitotic bodies (separating nuclei cells). It is because, MAI plays a vital part in evaluating the rate of cell proliferation, and it has a predictive importance in assessing cancer aggressiveness and BC grading [3]. Bloom-Richardson BC grading method has contained 3 features, but mitotic count (MC) is a vital measure when compared to others. Being a fragment of the BC grading method, the MC has also been measured as a separate analytical biomarker. So, it can be employed in order to describe the treatment procedure and project novel healing agents to handle the cell division path [4]. The foremost steps detected in typical histopathology are surgery of cancerous tissue, fixation of tissue on a slide of glass, stain utilizing Hematoxylin and Eosin (H&E) dye, assortment of areas of interest [5].

According to pathologists, the vision classification of mitotic nuclei (MN) is a biased and time-consuming challenge with worse accuracy owing to many tasks [6]. Generally, MN are hyper-chromatic entities with numerous morphological sizes and shapes. Furthermore, the rate of MN within a ten HPF differs depending upon the cancer stage and grade. In aggressive cancers, generally, MN grows in very small dimensions with the highest rate are non-different [7]. The accurate classification of MN is based on the knowledge of pathologists and skills. Object-level inter-observer research shows pathologists' differences on separate objects. Present growths in DCNN and their worthy solution for the classification of images, segmentation, and recognition have enhanced their usage in medicinal image concerns [8]. DCNNs are a kind of typical learning systems that mechanically remove the related data from raw imageries without placing struggle into the physical planning of feature descriptors. CNN-based techniques are efficiently useful in many histopathology problems with attainment, for example: classification of breast tissue into benign, normal, aggressive carcinoma, recognition of cancer metastasis, quantification of lymphocytes, separation of cancer area, division of cell nuclei, etc [9]. Likewise, many CNN-based systems are projected to identify mitosis; but these methods still have a boundary of development owing to the stimulating nature of the issue [10]. Automatic recognition of MN is a highly challenging task owing to their usual formation and alteration in the surface of cells in dissimilar morphological stages.

This study presents an Optimal Bayesian Neural Network based Decision Support System for Mitotic Nuclei Detection (OBNN-DSSMND) technique on HIs. In the initial phase, the OBNN-DSSMND technique undergoes the bilateral filtering (BF) technique to preprocess the input images. Next, the OBNN-DSSMND technique involves a feature fusion process encompassing SqueezeNet, DenseNet, and VGG-19 models. Meanwhile, the hyperparameter selection of the DL models is performed by using the Archimedes Optimization algorithm (AOA). For mitotic nuclei detection, the OBNN-DSSMND technique applies a BNN classifier, which recognizes the existence of mitotic and non-mitotic cells on the HIs. The experimental assessment of the OBNN-DSSMND methodology can be examined utilizing a benchmark image database.

2. Literature Review

Liu et al. [11] established a deep network model that comprises two sections. The system primarily develops an innovative patch learning technique; while the deep supervision method was presented to attain the coherent contributions in every scale layer. For improving nuclear localization, the technique develops an iterative correction approach to create the predictive increasingly near-the-ground truth that significantly increases the accuracy of nuclear localization and enables the choice of neighbor sizes. In [12], an optimization-based superpixel-clustering method has been developed. The image pre-processing could be achieved by implementing the normalization method. Later normalization and segmentation were executed by applying the superpixel with GWO and PSO for segmenting. Afterward, feature extractor has been executed through colour autocorrelogram, circularity, solidity, eccentricity, Local Direction Ternary Pattern (LDTP), perimeter, and GLCM. In conclusion, the Support Vector Machine (SVM) method has been employed. In [13], an Enhanced Pelican Optimizer Algorithm with a DL-Driven MN Classification (EPOADL-MNC) method was introduced. Similarly, the ShuffleNet architecture was utilized for the feature extraction technique. During the process of parameter tuning, the EPOADL-MNC method creates usage of the EPOA model for modifying the parameter tuning of the ShuffleNet architecture. Lastly, an ANFIS technique was deployed for classification and identification.

In [14], a two-phase cascaded network called FoCasNet was developed to identify the mitosis. During the primary phase, a detection model was developed for screening as many candidates as possible. In the secondary phase, a classification model was devised to improve the outcomes of the primary phase. Additionally, the hybrid anchor branch classification subnet, normalization technique, and attention mechanism have been presented for increasing the overall detection efficiency. The authors [15] presented an artificial hummingbird algorithm with a TL-based MN classification (AHBATL-MNC) method. For HI segmentation procedures, the PSPNet architecture has been employed to recognize the candidate mitotic patterns. Then, the ResNet has been exploited as a feature extractor, and the XGBoost algorithm can be executed. The hyperparameter tuning of the XGBoost system is executed with the help of the AHBA method. Ghaznavi et al. [16] projected a hybrid DL-based definite segmentation and classification technique. The inception component in the Inception-UNet confined kernels with various dimensions with similar layers for extracting each feature descriptor. The sequence of residual blocks with skip connections at every level of ResNet34-UNet lessened the gradient vanishing complexity and enhanced the generalization capability.

In [17], an advanced DCNN technique has been developed for nuclei detection, segmentation, and classification processes. The Recurrent Residual UNet (R2UNet) and R2UNet-based regression method called the University of Dayton Net (UD-Net) could be exploited for nuclei detection and segmentation processes correspondingly. In [18], a robust and generalizable mitosis detection technique (named as FMDet) was developed. The pixel-level interpretations for MN have been acquired by the correlation of the masks produced in a better-trained nuclear segmentation method. At the segmentation model, a strong feature extractor must be devised that was

made by incorporating a channel-specific multiple scale attention mechanism with a fully connected (FC) network model.

3. The Proposed Method

In this paper, we have presented an OBNN-DSSMND technique on HIs. The goal of the OBNN-DSSMND technique is to detect the mitotic and non-mitotic cells on the HIs. The OBNN-DSSMND technique contains a series of processes such as BF-based image preprocessing, feature fusion process, AOA-based parameter tuning, and BNN-based classification. Fig. 1 depicts the entire procedure of the OBNN-DSSMND methodology.

3.1. Preprocessing

In the initial phase, the OBNN-DSSMND technique undergoes the BF approach to preprocess the input images. BF is a nonlinear filtering algorithm utilized in image processing to decrease noise while retaining edges [19]. BF considers the similarity of spatial intensity and proximity between pixels, unlike classical linear filtering which smoothes equally each pixel. BF can efficiently remove noise while retaining image properties by applying a weighted average based on these factors, making it especially suitable in tasks like edge preservation and image denoising. This method finds application in different fields such as digital photography, computer vision, and medical imaging, where maintaining image detail and clarity is essential.

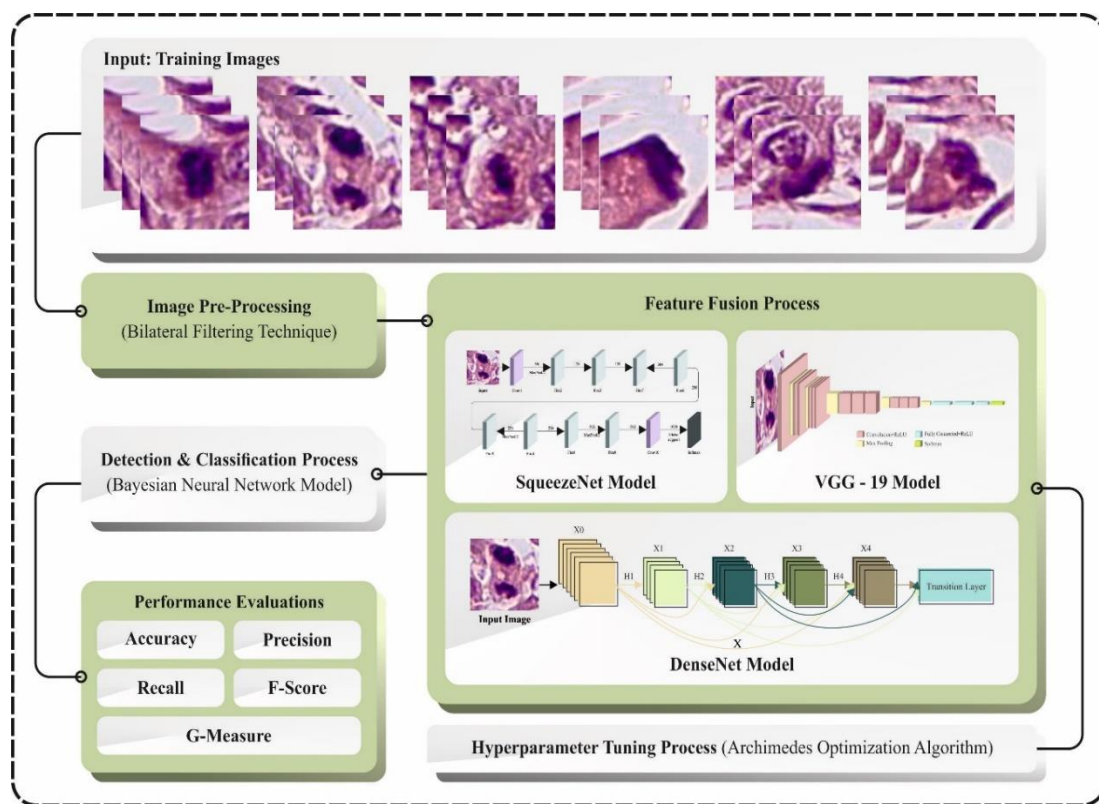


Figure 1. Overall procedure of OBNN-DSSMND technique

3.2. Feature Fusion Process

Next, the OBNN-DSSMND technique involves a feature fusion process encompassing SqueezeNet, DenseNet, and VGG-19 models.

3.2.1. SqueezeNet Model

As a variant of Deep Neural Network, SqueezeNet is constructed for image classification [20]. The objective is to preserve better accuracy levels, while they are smaller and more effective than other DNNs. SqueezeNet achieves efficiency and tiny size known as Network compression. SqueezeNet is used to replace the convolution layer that is expensive and large with dense and efficient ones. It achieves innovative application by incorporating pooling and 1×1 convolutional layers that can considerably reduce the quantity of variables. Furthermore, it is noteworthy that SqueezeNet encompasses a Fire Module. The Modules, which include expansion and squeeze layers, are the constituent elements of the network.

The size of the 1×1 convolution layer has been employed to decrease the input channel counts, while the sizes of 3×3 and 1×1 convolution layers are incorporated in the expansion layer to increase the number of output channels. Finally, the network efficiently gathers properties of local and global input images. Note that the Squeeze uses a deep supervision technique, which has the expansion of the network in addition to the classification layer. Multiple classification levels result in better model performance than an output classification.

SqueezeNet receives and predicts the model according to the features extracted from the data. Deep supervision can improve the model performance that proposes myriad classification layers. The SqueezeNet model has three different stages, the convolutional layer, eight Fire modules, and the ultimate convolution layer.

3.2.2. DenseNet Model

The unique principle of DenseNet keeps in its initial thought of a feed-forward network, donating upon is a noticeable power over other network structures [21]. DenseNet provides an excess of absorbing benefits. At primary, DenseNet aids in moderating the issue of vanishing gradient. In addition, DenseNet displays its ability by increasing the spread of features, raising their restoration, and efficiently decreasing the count of parameters. It is attained over the exclusive device of a dense layer that classily combines the output from the previous layer by linking them beside the depth element. The DenseNet procedure merges dense blocks and transition layers in order to sort an input review based on its substance. If a text can delivered as an input to DenseNet, then it is handled over numerous dense blocks. Every layer-mapping feature endure the similar from layer-wise but the filters alter from layer-wise in a particular dense block. Depending upon a dense block, data affecting DenseNet growth to the subsequent phase is called the transition layer.

In the DenseNet structure, the transition layer accepts the critical responsibility of performing dual important processes such as convolution (Conv) and pooling. These processes are carefully executed in the downsampling measures that are well-placed exterior of the dense blocks. During the DenseNet structure, the transition layer includes various modules such as batch normalization (BN) and other vital features like Conv and average pooling layers, all functioning jointly to enhance computation efficacy and to diminish the amount of input feature map. Afterward, a layer of average global pooling was executed, and outcomes were delivered to a classifier of Softmax.

3.2.3. VGG-19 Model

VGG19 is a CNN version of VGG16 developed for image classification [22]. It takes three FC layers, comprising sixteen convolution (conv) layers and nineteen layers. Assume X is the input image tensor with sizes $H \times W \times C$, where H , W , and C signify height, width, and channels correspondingly (for example RGB pictures). VGG19's 1st layer is a conv layer with 64 filters, every dimension $3 \times 3 \times 3$ (3×3 defines the filter dimension and 3 has the channel counts from the input images).

Assume F_1 is the group of filters. The output will be denoted as:

$$V_1 = ReLU(Conv(X, F_1) + b_1) \quad (1)$$

In this context, b_1 denotes the bias, $ReLU$ means the rectified linear activation function, and 'conv ()' indicates the operation of convolution. Next, the CL with 64 filters, followed by a MaxPoolLayer (MPL). The resultant of the layer will be given below:

$$V_2 = MaxPool(ReLU(Conv(Z_1, F_2) + b)) \quad (2)$$

Here b_2 represents the bias term, F_2 means the filter set, $max_pool()$ refers to the max pooling function, and. Other layers in VGG19 follow the same pattern of modifying conv and MPLs. The conv layers like 128, 256, 512, and 512 filters within the next 4 layers, correspondingly, and every dimension of filters is $3 \times 3 \times M$ in which M refers to the channel counts in the preceding layer. Apart from these CLs, VGG19 features, 3 FC layers, every with 4096 neurons. Lastly, the SM layer with output neurons is equivalent to the categorization assignment number of classes. The outcome from the final FC layer will be represented as:

$$Z_F = ReLU((W_F * Flatten(Z_{Conv5})) + b_F) \quad (3)$$

Where b_F defines the bias term, W_F means the weight matrix that can be connected to the FC layer, and $fatten()$ refers to the process that fattens the output of the preceding layer to a vector. Also, the resultant of the SM layer will be denoted as:

$$Y_{(SM)} = SoftMax (W_{SM} * Z_F) + b_{SM} \tag{4}$$

Here b_{SM} defines the bias term, and W_{SM} describes the weight matrix that is linked to the softmax layer to the preceding layer. The $SoftMax()$ function standardizes the output to a probability distribution through the class labels. The major variance between VGG19 and VGG16 is the amount of conv layers. VGG19 takes 3 added conv layers with 128, 256, and 512 filters, individually, when related to VGG16. The deeper network permits additional intricate features that should be learned and improved effectiveness under the specified image classification methods.

3.3. Hyperparameter Tuning using AOA

At this phase, the hyperparameter selection of the DL models is performed by using the AOA. The AOA is a state-of-the-art metaheuristic optimization method that dependent upon Archimedes’ buoyancy principle’s physical principles [23]. The object’s location has been upgraded by simulating the object method progressively showing neutral buoyancy succeeding a collision. The AOA method offers a specific population by submerging objects with acceleration, density, and volume features. The product must determine its place in the fluid reliant on these aspects. The AOA upgrades the density, acceleration, and volume of objects in the optimization process. The object’s place will be updated in accordance with its individual abilities. During Initialization, upgrading object features, upgrading the position of object, and calculation is an important process for stages of the AOA.

Initialized of the place and features of the object can be derived as given below:

$$X_i = lb_i + rand() \cdot (ub_i - lb_i), \tag{5}$$

Here The variable $rand()$ is a d-dimensional vector produced arbitrarily in the range of [0,1], X_i represents a candidate solution vector i^{th} of object population dimension $N, i = 1,2, \dots, N$, and the limitations lb_i and ub_i describe the lower and upper bounds, correspondingly. The i -th object variables of acceleration are denoted as c_i , volume is represented as vo_i , and density is indicated as de_i , correspondingly; $vo_j = rand$, $de_i = rand$, and $acc_i = lb_i + rand() \cdot (ub_i - lb_i)$. The attributes and place of the optimum object such as $vo_{best}, X_{best}, de_{best}$, and ac_{best} —have been chosen objects with the top fitness values based on the computation of every object.

Object properties stage: At the iteration, the object’s density and volume were upgraded as per the given mathematical Eqs (6) – (7):

$$vo_i^{t+1} = vo_i^t + rand \cdot (vo_{best} - vo_i^t), \tag{6}$$

$$de_i^{t+1} = de_i^t + rand \cdot (de_{best} - de_i^t), \tag{7}$$

Here de_i^{t+1} and vo_i^{t+1} describes the density and volume of the i^{th} object at the iteration $t + 1$. The virtual collisions among objects at the AOA have been imitated to the Eq. (9) optimization method; the method progressively gets equilibrium. A transform variable should be employed as a method to simulate accomplishing the transformation of model in the searching exploration to exploitation as represented by:

$$TP = \exp\left(\frac{t - t_{max}}{t_{max}}\right) \tag{8}$$

whereas TF denotes the transform variable, t and t_{max} describes the existing number of iterations and maximum iterations, correspondingly TF slowly rising to 1 over time. $TP \leq 0.5$ defines one second of iteration under the exploration stage. The object features of upgrade acceleration can be compared with the collision objects.

$$ac_i^{t+1} = \begin{cases} \frac{de_{mr} + vo_{mr} \cdot ac_{mr}}{de_i^{t+1} \cdot vo_i^{t+1}}, & \text{if } TF \leq 1/2 \\ \frac{de_{best} + vol_{best}^i \cdot ac_{best}}{de_i^{t+1} \cdot vo_i^{t+1}}, & \text{otherwise} \end{cases} \tag{9}$$

Now, de_{mr} , vo_{mr} , and ac_{mr} represent the density, volume, and acceleration of random material (mr), correspondingly. When $TP \leq 0.5$, it will be a collision amongst objects, and mathematical equations for acceleration upgrades of object i at iteration t ; or else, without any collisions among objects. The standardization approach for the acceleration will be upgraded as given below:

$$ac_{i,norm}^{t+1} = ur \cdot \frac{ac_i^{t+1} - \min(ac)}{\max(ac) - \min(ac)} + lr, \quad (10)$$

Here $ac_{i,norm}^{t+1}$ characterizes the standardized acceleration of i -th object with respect to the $t + 1$ iteration. The ur and lr describe the normalized values that can be set to 0.8 and 0.2, correspondingly.

Upgrading the place of objects must be executed in this way: When $TF \leq 1/2$ (exploration stage), the location upgrade equation of object i in the iteration $t + 1$ will be useful for searching at global to local and region of converge wherein the optimum outcome occurs; alternatively, it will be a searching exploitation stage in the location upgrading. Once the object is different from the best place, the acceleration values will be large, and the object will exist at the exploration stage. If the values of acceleration are smaller, the object could be close to the optimum outcome. The exploitation stage will be explained in a detailed manner:

$$X_i^{t+1} = X_i^t + C_1 \cdot rand \cdot ac_{i,norm}^{t+1} \cdot d \cdot (X_{rand} - X_i^t) \quad (11)$$

whereas C_1 refers to a constant as a set of 2, and d means the density parameter that reduces with respect to time like $d = \exp\left(\frac{t-t_{max}}{t_{max}}\right) - \left(\frac{t}{t_{max}}\right)$. The acceleration modifies from larger to smaller, representing the method's change from exploration to exploitation, correspondingly can support the object methodology and optimum global solution.

$$X_i^{t+1} = X_{best}^t + F \cdot C_2 \cdot rand \cdot ac_{i,norm}^{t+1} \cdot d \cdot (T \cdot X_{best} - X_i^t) \quad (12)$$

Now F means the direction of motion, C_2 characterizes the constant t ; T defines the variable proportional to the transfer purpose—the percentage utilized for achieving the optimum place - $T = C_3 \times TP$; and the mathematical formula will be represented by:

$$F = \begin{cases} +1, & \text{if } P \leq 0.5 \\ -1, & \text{if } P > 0.5 \end{cases} \quad (13)$$

We know that P is fixed to $2 \cdot rand - C_4$.

Calculating the main function includes the computation of fitness values for the main function and then upgrading the location of the object at every iterative time. The algorithm with the main function has been applied in fitness value assessment by analyzing every object to be detailed with the values of best fitness determined at every location, for example, ac_{best} , de_{best} , X_{best} , and vo_{best} are upgraded for the following generations or iterations.

The fitness choice is a key aspect controlling the solution of AOA. The parameter solution procedure contains the encoded performance to measure the effectiveness of the candidate outcomes. During this case, the AOA assumes that accuracy is the main condition to design the fitness function (FF) that can expressed as:

$$Fitness = \max(P) \quad (14)$$

$$P = \frac{TP}{TP + FP} \quad (15)$$

where TP and FP demonstrate the true and false positive rates.

3.4. Mitotic Nuclei Detection using BNN Model

At last, the OBNN-DSSMND technique applies a BNN classifier, which recognizes the presence of mitotic and non-mitotic cells on the HIs for mitotic nuclei detection. A BNN is a method of ANN that unites the versatility and flexibility of ANN, with the capability to manage the insecurity of the parameter [24]. It creates the probability distribution utilizing Bayesian inference, as tackled to estimates, different standard ANNs. This permits BNN to include insecurity in their forecasts and deliver additional precise outcomes. BNN was executed in a wide range of applications like reinforcement learning, natural language processing (NLP), and image classification.

Murat describes the Bayesian structure for neural networks; his tactic concentrates on the probabilistic analyses of system structures. On the other hand, in conventional network training, the optimal weights were gained by diminishing the function of error; the Bayesian tactic uses a probability distribution of the system weight. Therefore, the common system's forecast is dependent upon a probability distribution. During the theory of Bayesian, the weights can be randomly generated and their posterior distribution is adapted as per the rule of Bayes. Fig. 2 represents the infrastructure of BNN.

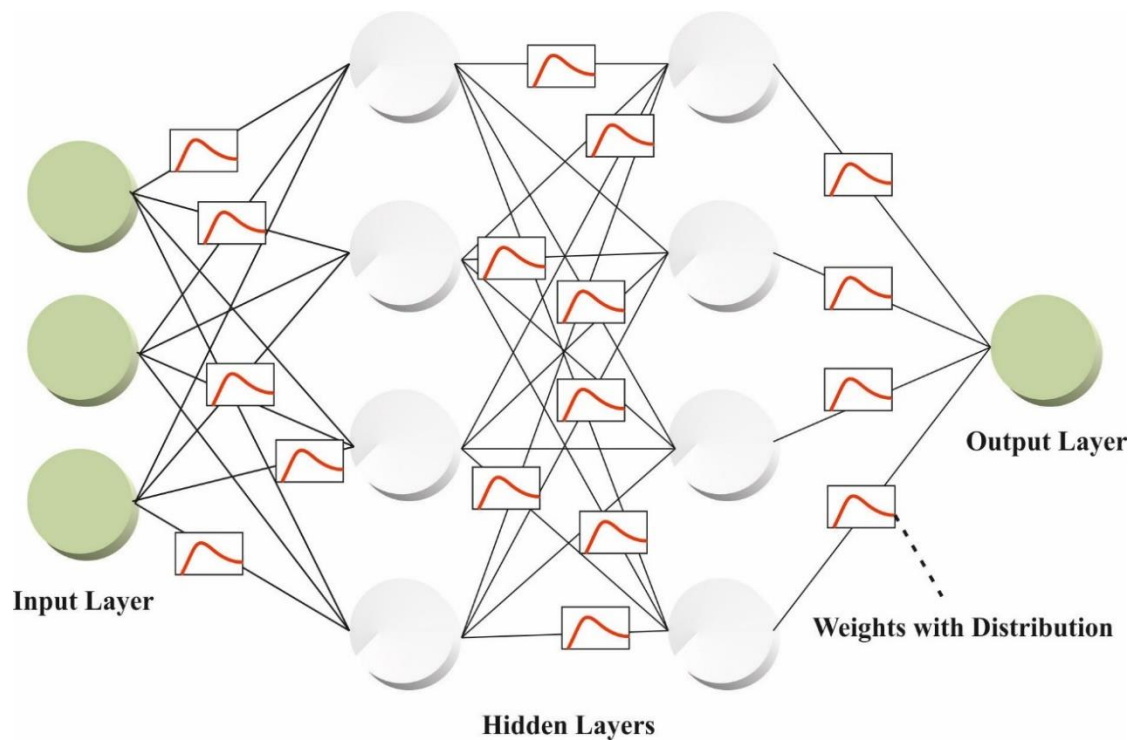


Figure 2. Structure of BNN

Therefore, the calculation is as below.

$$k(\omega|C, \alpha, \beta, L) = \frac{K(C|\omega, \beta, L)K(\omega|\alpha, L)}{K(C|\alpha, \beta, L)} \quad (16)$$

Here, the foremost neural networks method is signified as K , the sample of training is denoted as C , the weight distribution is defined as $k(\omega|\alpha, L) = \left(\frac{\alpha}{2\pi}\right)^{\frac{m}{2}} \exp\left\{-\frac{\alpha}{2}\omega^1\omega\right\}$, L is one of the specific ANNs, and ω is the vector with their weights. $K(\omega|\alpha, L)$ defines the foremost layer of data before the intended data are composed, and $K(C|\omega, \beta, L)$ refers to the parallel function that is the prospect of the data arising assuming the weight. The posterior calculation is definite in Eq. (17).

$$Posterior = \frac{Likelihood \times prior}{Evidence} \quad (17)$$

A BNN generates probabilistic assurances for its forecasts, and the parameter distribution has been acquired from the remarks. Therefore, one can develop the kind and procedure neural network from space. These dual features make BNNs smart to both practitioners and theorists.

4. Performance Validation

The experimental assessment of the OBNN-DSSMND approach can be examined utilizing a benchmark image dataset [25]. It takes 150 images with 2 classes as illustrated in Table 1. Fig. 3 exemplifies the sample images.

Table 1: Details on database

Classes	No. of Images
Mitosis	75
Nonmitosis	75
Total No. of Images	150

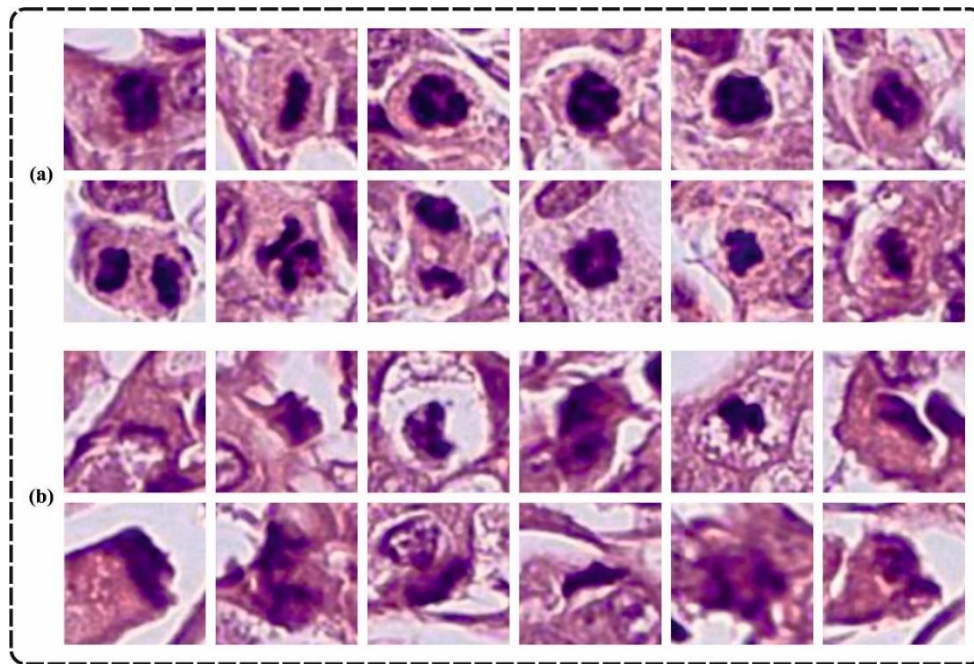


Figure 3. Sample images

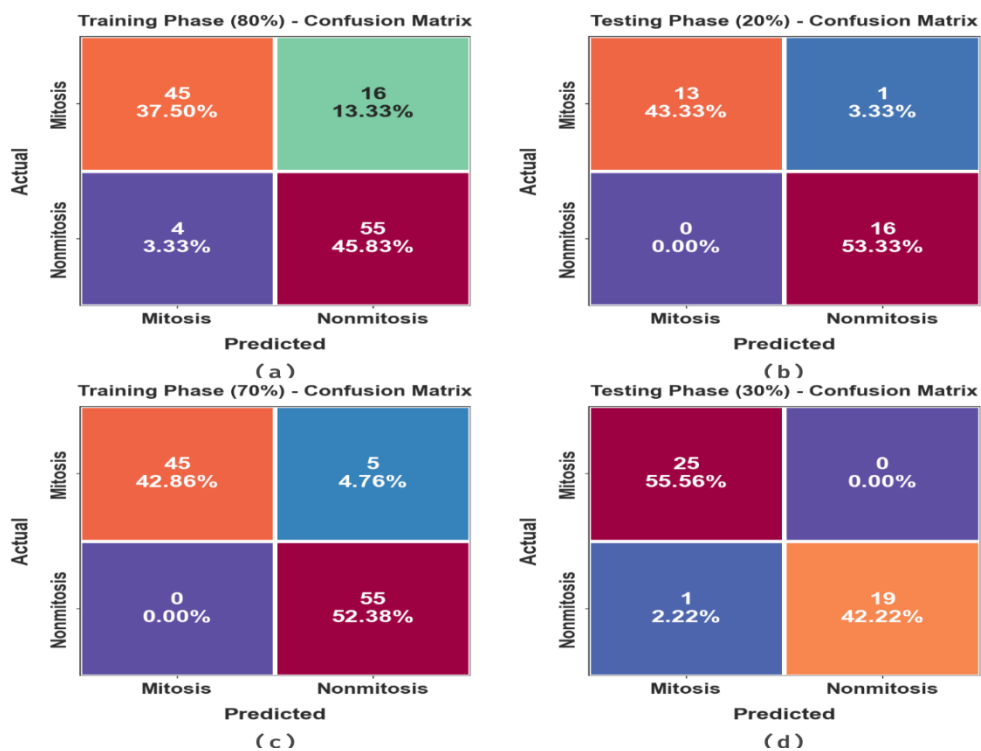


Figure 4. Confusion matrices of (a-b) 80:20 of TRAST/TESST and (c-d) 70:30 of TRAST/TESST

Fig. 4 displays the confusion matrices developed by the OBNN-DSSMND methodology at 80:20 and 70:30 of TRAST/TESST. These outcomes denote that the OBNN-DSSMND algorithm has effectual recognition and classification of mitosis and non-mitosis classes.

The mitotic nuclei detection results of the OBNN-DSSMND system can be considered with 80%TRAST and 20%TESST in Table 2 and Fig. 5. These experimental outcomes implied that the OBNN-DSSMND method recognizes different two classes under mitosis and non-mitosis. With 80%TRAST, the OBNN-DSSMND methodology offers an average $accu_y$ of 83.50%, $prec_n$ of 84.65%, $reca_t$ of 83.50%, F_{score} of 83.22%, and

$G_{measure}$ of 83.64%. Besides, with 20% TESST, the OBNN-DSSMND algorithm achieves an average $accu_y$ of 96.43%, $prec_n$ of 97.06%, $reca_l$ of 96.43%, F_{score} of 96.63%, and $G_{measure}$ of 96.69%, respectively.

Table 2: Mitotic nuclei recognition outcome of OBNN-DSSMND methodology with 80% TRAST and 20% TESST

Classes	$Accu_y$	$Prec_n$	$Reca_l$	F_{Score}	$G_{Measure}$
TRAST (80%)					
Mitosis	73.77	91.84	73.77	81.82	82.31
Nonmitosis	93.22	77.46	93.22	84.62	84.98
Average	83.50	84.65	83.50	83.22	83.64
TESST (20%)					
Mitosis	92.86	100.00	92.86	96.30	96.36
Nonmitosis	100.00	94.12	100.00	96.97	97.01
Average	96.43	97.06	96.43	96.63	96.69

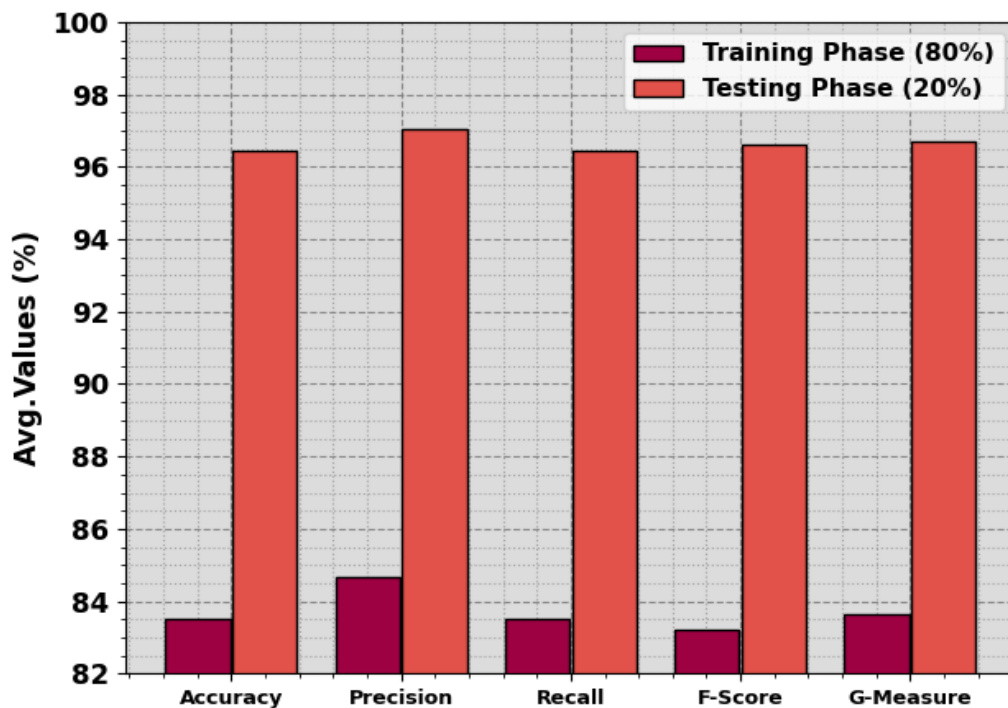


Figure 5. Average of OBNN-DSSMND technique with 80% TRAST and 20% TESST

The mitotic nuclei detection outcomes of the OBNN-DSSMND method have been examined with 70% TRAST and 30% TESST in Table 3 and Fig. 6. These attained values emphasized that the OBNN-DSSMND method recognizes diverse two classes with mitosis and non-mitosis. According to 70% TRAST, the OBNN-DSSMND method gains an average $accu_y$ of 95.00%, $prec_n$ of 95.83%, $reca_l$ of 95.00%, F_{score} of 95.19%, and $G_{measure}$ of 95.31%. Meanwhile, based on 30% TESST, the OBNN-DSSMND algorithm accomplishes an average $accu_y$ of 97.50%, $prec_n$ of 98.08%, $reca_l$ of 97.50%, F_{score} of 97.74%, and $G_{measure}$ of 97.76%.

Table 3: Mitotic nuclei detection outcome of OBNN-DSSMND technique with 70%TRAST and 30%TESST

Classes	$Accu_y$	$Prec_n$	$Reca_t$	F_{Score}	$G_{Measure}$
TRAST (70%)					
Mitosis	90.00	100.00	90.00	94.74	94.87
Nonmitosis	100.00	91.67	100.00	95.65	95.74
Average	95.00	95.83	95.00	95.19	95.31
TESST (30%)					
Mitosis	100.00	96.15	100.00	98.04	98.06
Nonmitosis	95.00	100.00	95.00	97.44	97.47
Average	97.50	98.08	97.50	97.74	97.76

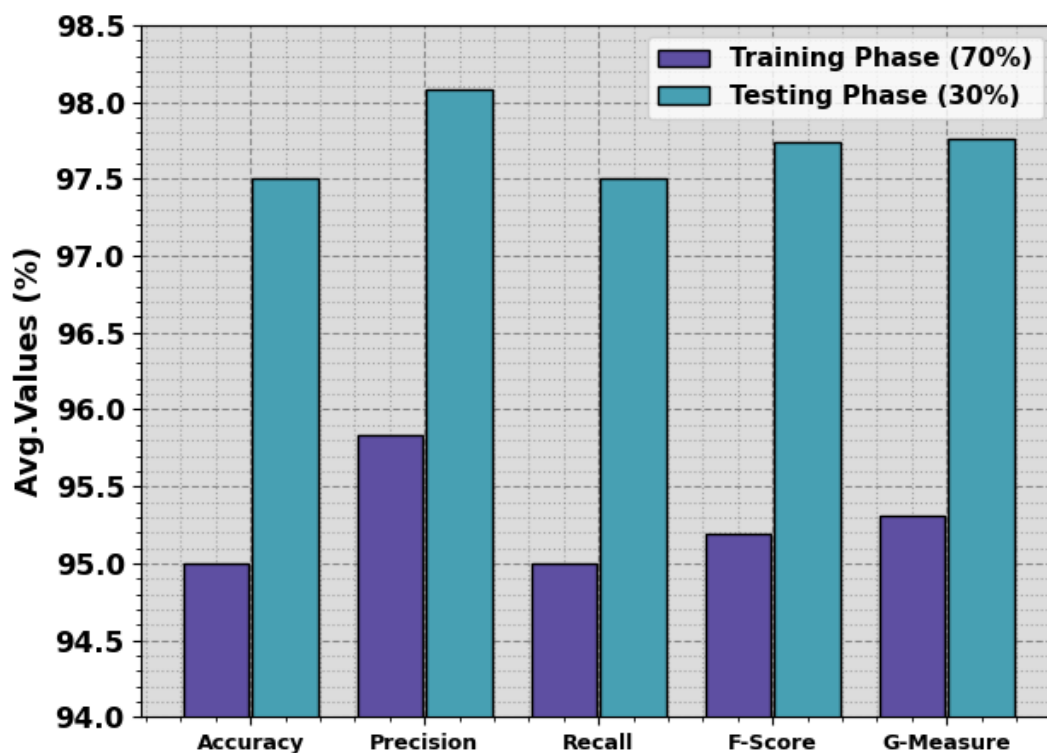


Figure 6. Average of OBNN-DSSMND technique at 70%TRAST and 30%TESST

The efficiency of the OBNN-DSSMND methodology is graphically projected in Fig. 7 in the procedure of training accuracy (TRAAC) and validation accuracy (VALAC) curves with 70%TRAST and 30%TESST. The outcome displays a useful investigation of the behaviour of the OBNN-DSSMND algorithm at distinct count of epochs, representing its learning method and generalized abilities. Primarily, the outcome denotes a constant enhancement in the TRAAC and VALAC with progress in epochs. It ensures the adaptive nature of the OBNN-DSSMND technique in the pattern identification method under both data. The improved trends in VALAC outline the ability of the OBNN-DSSMND method to adjust to the TRA set and surpass to provide correct classification of undetected data, demonstrating robust generalized capabilities.

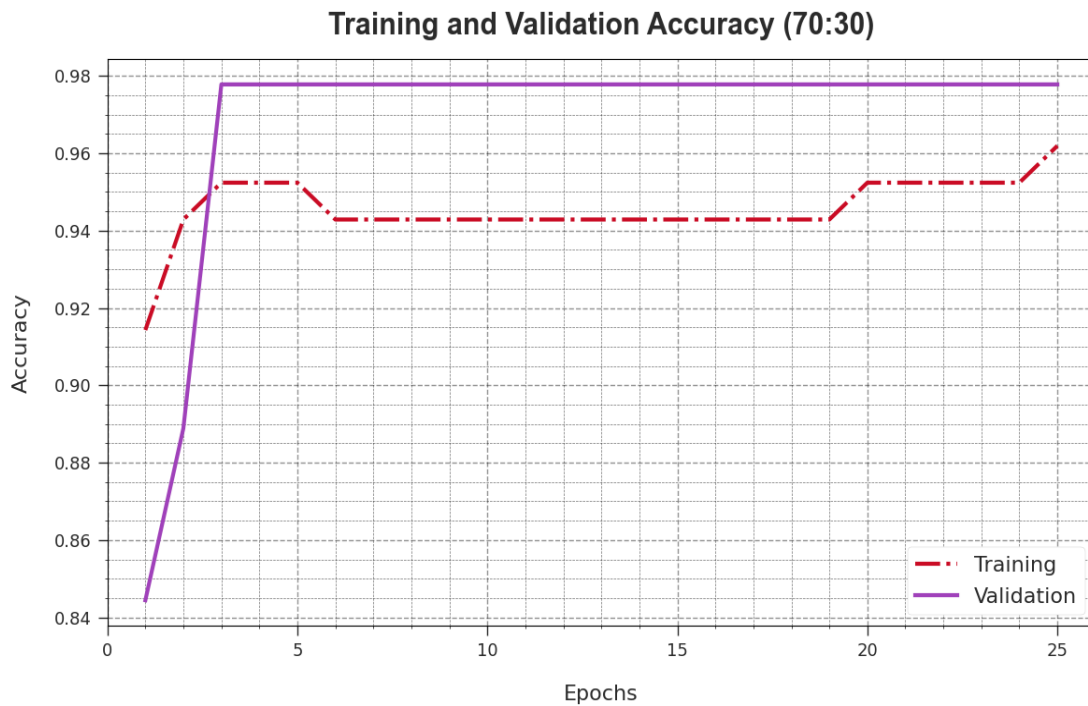


Figure 7. $Accu_y$ curve of OBNN-DSSMND technique with 70% TRAST and 30% TESST

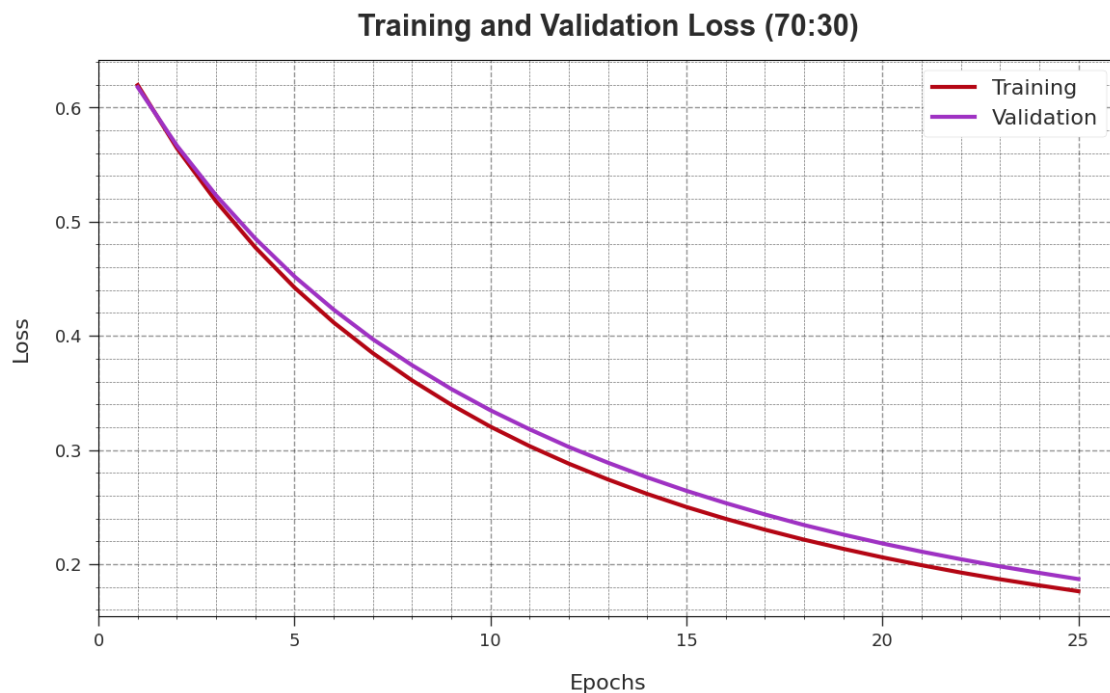


Figure 8. Loss curve of OBNN-DSSMND algorithm under 70% TRAST and 30% TESST

Fig. 8 shows a complete outline of the training loss (TRALS) and validation loss (VALLS) results of the OBNN-DSSMND method over distinct epochs with 70% TRAST and 30% TESST. The progressive minimization in TRALS outperforms the OBNN-DSSMND methodology enhancing the weights and decreasing the classifier error at both data. The outcome specifies a clear knowledge of the OBNN-DSSMND method connected to the TRA data, highlighting its ability in capturing patterns. Mostly, the OBNN-DSSMND system incessantly increases its parameters in decreasing the variances among the actual and predictive TRA class labels.

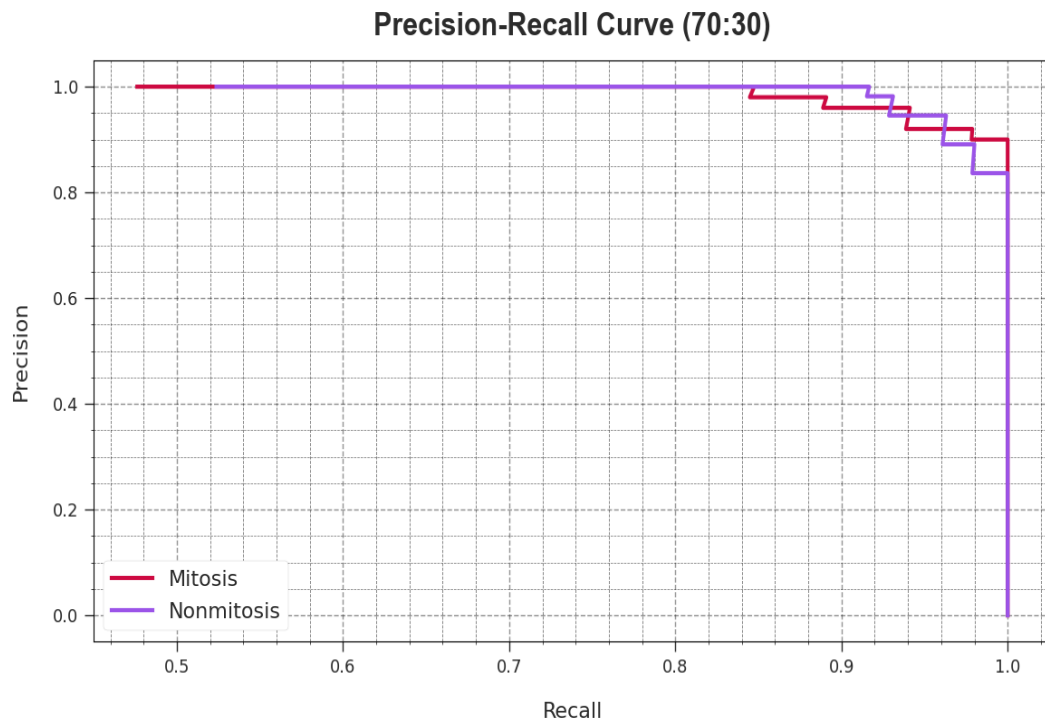


Figure 9. PR curve of OBNN-DSSMND methodology at 70%TRAST and 30%TESST

Examining the PR curve, as displayed in Fig. 9, the outcomes ensured that the OBNN-DSSMND system gradually attains improved PR rates at each class with 70%TRAST and 30%TESST. It confirms the enriched abilities of the OBNN-DSSMND algorithm in the identification of distinct classes, showing ability in the recognition classes.

Similarly, in Fig. 10, ROC curves acquired by the OBNN-DSSMND methodology exhibited the classification of distinct labels with 70%TRAST and 30%TESST. It gives a widespread data of the tradeoff between TPR as well as FRP over distinct recognition threshold values and count of epochs. The outcome emphasized the higher classifier results of the OBNN-DSSMND algorithm with every class, outlining the efficacy in overcoming several classification issues.

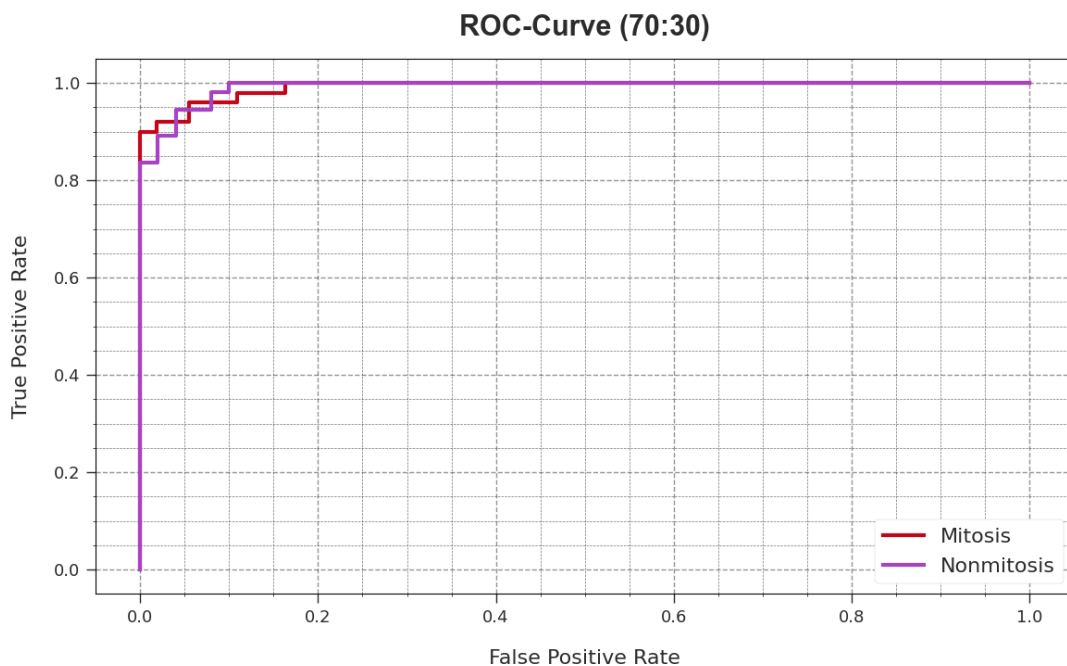


Figure 10. ROC curve of OBNN-DSSMND model with 70%TRAST and 30%TESST

To ensure the mitotic nuclei detection assessment of the OBNN-DSSMND method, a wide-ranging comparative outcome is stated in Table 4 and Fig. 11 [15]. These experimentation outcome values result from the display that the VGG16 method has shown poorer performance with decreased values. Likewise, the ResNext-50, Inception-V3, ResNet-18, DenseNet-201, DHE-Mit, and AHBATL-MNC algorithm have described closer values. But, the OBNN-DSSMND algorithm achieves superior outcomes with $accu_y$ of 97.50%, $prec_n$ of 98.08%, $reca_l$ of 97.50%, and F_{score} of 97.74%.

Table 4: Comparative outcomes of OBNN-DSSMND technique with recent models

Methods	$Accu_y$	$Prec_n$	$Reca_l$	F_{Score}
OBNN-DSSMND	97.50	98.08	97.50	97.74
AHBATL-MNC	96.79	96.79	96.79	96.68
DHE-Mit	86.85	86.12	76.95	79.02
DenseNet-201 Model	85.47	84.80	75.48	77.95
ResNet-18 Model	83.67	82.96	73.28	75.78
Inception-V3 Model	80.07	79.14	69.69	72.29
ResNext-50 Model	79.11	77.78	68.52	71.17
VGG-16 Model	76.49	75.49	66.60	69.27

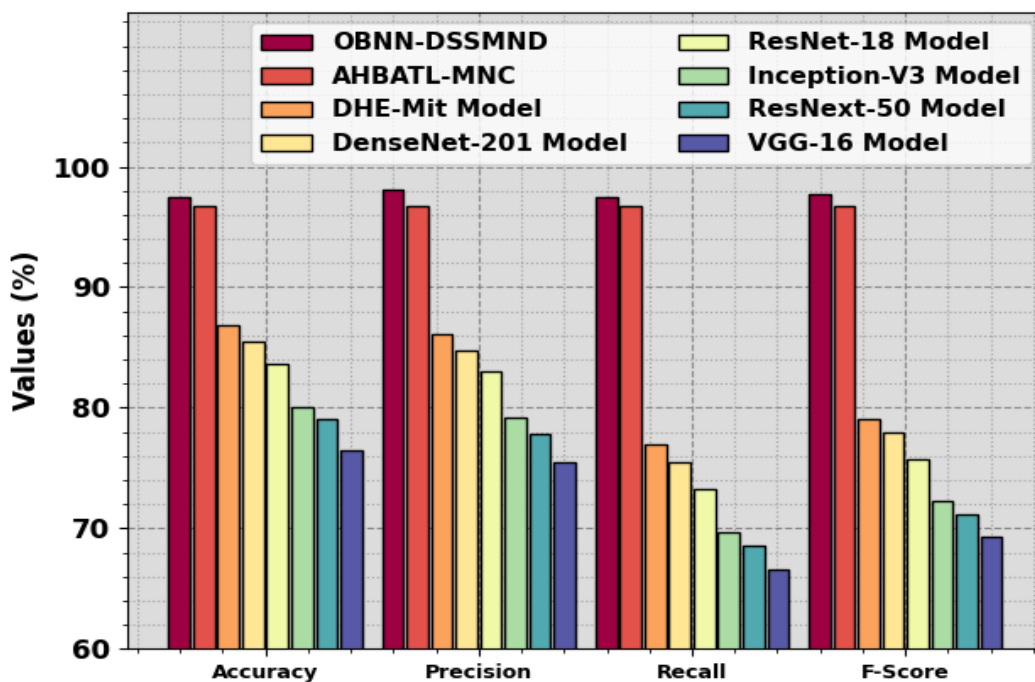


Figure 11. Comparative analysis of OBNN-DSSMND technique with other models

To examine the mitotic nuclei detection assessment of the OBNN-DSSMND method, an extensive comparative computational time (CT) outcome is reported in Table 5 and Fig. 12. These experimentation outcomes represent that the VGG16 technique gets the lowest performance with increased values.

Table 5: CT outcome of OBNN-DSSMND technique with recent other algorithms

Methods	Computational Time (s)
OBNN-DSSMND	8.11
AHBATL-MNC	12.36
DHE-Mit	25.19
DenseNet-201	42.60
ResNet-18	41.05
Inception-V3	59.69
ResNext-50	39.38
VGG-16	56.16

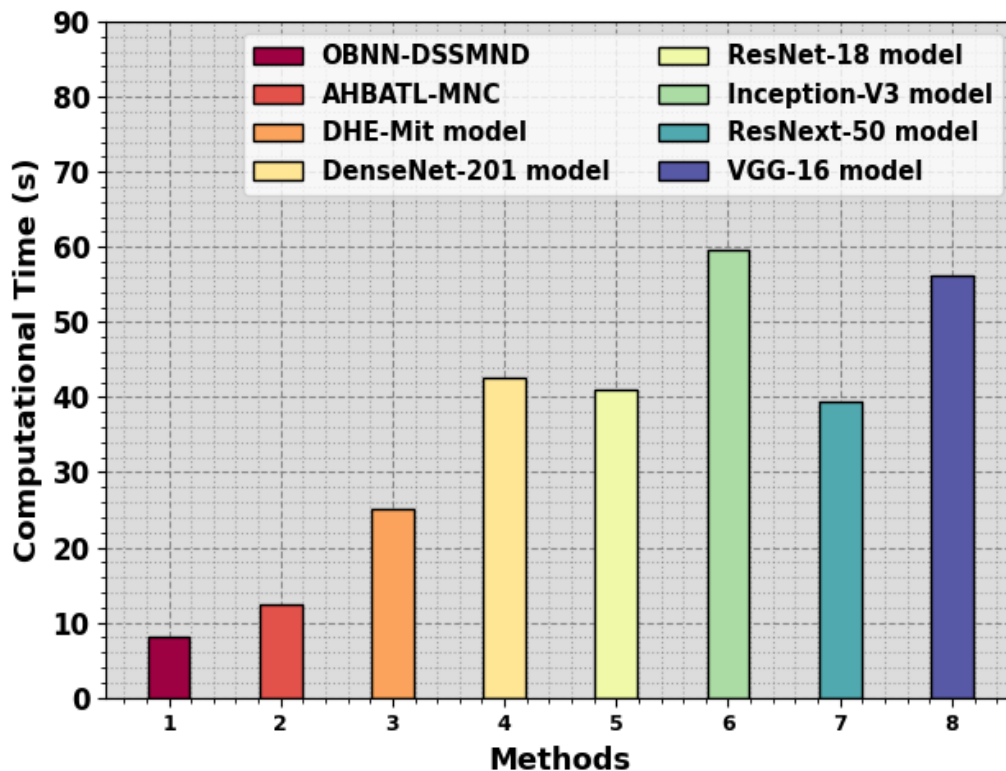


Figure 12. CT analysis of OBNN-DSSMND technique with other models

Alternatively, the ResNext-50, Inception-V3, ResNet-18, DenseNet-201, DHE-Mit, and AHBATL-MNC methods have been denoted as significant values. Nevertheless, the OBNN-DSSMND system achieves enhanced performance with a lessened CT of 8.11s, respectively.

5. Conclusion

In this study, we have presented an OBNN-DSSMND technique on HIs. The goal of the OBNN-DSSMND technique is to detect the mitotic and non-mitotic cells on the HIs. In the initial phase, the OBNN-DSSMND technique undergoes the BF technique to preprocess the input images. Next, the OBNN-DSSMND technique involves a feature fusion process encompassing SqueezeNet, DenseNet, and VGG-19 models. Meanwhile, the

hyperparameter selection of the DL models is performed by using the AOA. For mitotic nuclei detection, the OBNN-DSSMND technique applies a BNN classifier, which recognizes the presence of mitotic and non-mitotic cells on the HIs. The experimental assessment of the OBNN-DSSMND technique can be examined utilizing a benchmark image database. The widespread simulation analysis reported that the OBNN-DSSMND technique achieves better results than other techniques.

Data Availability Statement: The authors confirm that the data supporting the findings of this study are available within the article [25].

References

- [1] D. K. Das and P. K. Dutta, "Efficient automated detection of mitotic cells from breast histological images using deep convolution neural network with wavelet decomposed patches," *Computers in Biology and Medicine*, vol. 104, pp. 29–42, 2019.
- [2] K. S. Beevi, M. S. Nair, and G. R. Bindu, "Automatic mitosis detection in breast histopathology images using convolutional neural network-based deep transfer learning," *Biocybernetics and Biomedical Engineering*, vol. 39, pp. 214–223, 2019.
- [3] I. O. Sigirci, A. Albayrak, and G. Bilgin, "Detection of mitotic cells in breast cancer histopathological images using deep versus handcrafted features," *Multimedia Tools and Applications*, vol. 81, pp. 13179–13202, 2022.
- [4] T. Mahmood, M. Arsalan, M. Owais, M. B. Lee, and K. R. Park, "Artificial intelligence-based mitosis detection in breast cancer histopathology images using faster R-CNN and deep CNNs," *Journal of Clinical Medicine*, vol. 9, no. 749, 2020.
- [5] D. Cai, X. Sun, N. Zhou, X. Han, and J. Yao, "Efficient mitosis detection in breast cancer histology images by RCNN," in *Proc. IEEE 16th Int. Symp. Biomedical Imaging (ISBI)*, Venice, Italy, 2019, pp. 919–922.
- [6] N. Maroof et al., "Mitosis detection in breast cancer histopathology images using hybrid feature space," *Photodiagnosis and Photodynamic Therapy*, vol. 31, p. 101885, 2020.
- [7] C. Li et al., "Weakly supervised mitosis detection in breast histopathology images using concentric loss," *Medical Image Analysis*, vol. 53, pp. 165–178, 2019.
- [8] B. Lakshmanan, S. Priyadharsini, and B. Selvakumar, "Computer-assisted mitotic figure detection in histopathology images based on the DenseNet-PCA framework," *Materials Today: Proceedings*, vol. 62, pp. 4936–4939, 2022.
- [9] A. Sohail et al., "Deep object detection-based mitosis analysis in breast cancer histopathological images," *arXiv*, vol. 2003.08803, 2020.
- [10] A. A. Samah et al., "Mitotic cells detection in H&E-stained breast carcinoma images," *International Journal of Biomedical Engineering and Technology*, vol. 40, pp. 54–69, 2022.
- [11] Z. Liu, Y. Cai, and Q. Tang, "Nuclei detection in breast histopathology images with iterative correction," *Medical & Biological Engineering & Computing*, vol. 62, no. 2, pp. 465–478, 2024.
- [12] R. Satri and P. Chand Parvataneni, "Histopathology breast cancer detection and classification using optimized superpixel clustering algorithm and support vector machine," *Journal of the Institution of Engineers (India): Series B*, vol. 103, no. 5, pp. 1589–1603, 2022.
- [13] F. Alrowais et al., "Enhanced pelican optimization algorithm with deep learning-driven mitotic nuclei classification on breast histopathology images," *Biomimetics*, vol. 8, no. 7, p. 538, 2023.
- [14] H. Wang et al., "A novel dataset and a two-stage mitosis nuclei detection method based on a hybrid anchor branch," *Biomedical Signal Processing and Control*, vol. 87, p. 105374, 2024.
- [15] A. A. Malibari et al., "Artificial hummingbird algorithm with transfer-learning-based mitotic nuclei classification on histopathologic breast cancer images," *Bioengineering*, vol. 10, no. 1, p. 87, 2023.
- [16] A. Ghaznavi et al., "Symmetry breaking in the U-Net: Hybrid deep-learning multi-class segmentation of HeLa cells in reflected light microscopy images," *Symmetry*, vol. 16, no. 2, p. 227, 2024.
- [17] Z. Alom et al., "Microscopic nuclei classification, segmentation, and detection with improved deep convolutional neural networks (DCNN)," *Diagnostic Pathology*, vol. 17, no. 1, p. 38, 2022.
- [18] X. Wang et al., "A generalizable and robust deep learning algorithm for mitosis detection in multicenter breast histopathological images," *Medical Image Analysis*, vol. 84, p. 102703, 2023.
- [19] G. Wu, S. Luo, and Z. Yang, "Optimal weighted bilateral filter with dual-range kernel for Gaussian noise removal," *IET Image Processing*, vol. 14, no. 9, pp. 1840–1850, 2020.

- [20] R. Duan, D. Lin, and G. Fathi, "PEMFC model identification using a SqueezeNet developed by modified transient search optimization algorithm," *Heliyon*, vol. 10, p. 105374, 2024.
- [21] N. Ayub et al., "An efficient optimized DenseNet model for aspect-based multi-label classification," *Algorithms*, vol. 16, no. 12, p. 548, 2023.
- [22] K. S. Rao et al., "Intelligent ultrasound imaging for enhanced breast cancer diagnosis: Ensemble transfer learning strategies," *IEEE Access*, 2024.
- [23] T. K. Dao et al., "An optimal WSN node coverage based on enhanced Archimedes optimization algorithm," *Entropy*, vol. 24, no. 8, p. 1018, 2022.
- [24] Y. Fissaha et al., "Application of Bayesian neural network (BNN) for the prediction of blast-induced ground vibration," *Applied Sciences*, vol. 13, no. 5, p. 3128, 2023.
- [25] M. Veta et al., "Tumor proliferation assessment challenge 2016, MICCAI Grand Challenge," *MICCAI Grand Challenge*, 2016. [Online]. Available: <https://tupac.grand-challenge.org/>.